



Design and preparation of proline, tryptophan and poly-L-lysine functionalized magnetic nanoparticles and their radiolabeling with ^{131}I and ^{177}Lu for potential theranostic use

Marija Mirković^{a,*}, Zorana Milanović^a, Marko Perić^a, Sanja Vranješ-Đurić^a, Miloš Ognjanović^a, Bratislav Antić^a, Milorad Kuraica^b, Ivan Krstić^b, Martina Kubovcikova^c, Iryna Antal^c, Radka Sobotova^c, Vlasta Zavisova^c, Alena Jurikova^c, Martin Fabian^d, Martina Koneracka^c

^a Vinča^a Institute of Nuclear Sciences - National Institute of the Republic of Serbia, University of Belgrade, 11001 Belgrade, Serbia

^b Faculty of Physics, University of Belgrade, Studentski Trg 12, 11001 Belgrade, Serbia

^c Institute of Experimental Physics Slovak Academy of Sciences, Watsonova 47, 040 01 Kosice, Slovakia

^d Institute of Geotechnics Slovak Academy of Science, Watsonova 47, 040 01 Kosice, Slovakia

ARTICLE INFO

Keywords:

Amino acid-functionalized magnetic nanoparticles
Hyperthermia
Laser transmittance
Radiolabeling
Biodistribution

ABSTRACT

Surface modification of magnetic nanoparticles with poly-L-lysine, proline, and tryptophan was used to design potential theranostic agents for the application in cancer diagnosis and radionuclide-hyperthermia therapy. Characterization of bare and functionalized magnetic nanoparticles was performed in detail. The transparency of the examined magnetic nanoparticles was measured in the non-alternating magnetic field for a complete and better understanding of hyperthermia. For the first time amino acid-functionalized magnetic nanoparticles were labeled with theranostic radionuclides ^{131}I and ^{177}Lu . The specific absorption rate (SAR) procured for poly-L-lysine functionalized magnetic nanoparticles (SAR values of 99.7 W/g at $H_0 = 15.9$ kA/m and resonant frequency of 252 kHz) demonstrated their possible application in magnetic hyperthermia. Poly-L-lysine functionalized magnetic nanoparticles labeled with ^{177}Lu showed the highest radiochemical purity (>99.00 %) and *in vitro* stability in saline and serum (>98.00 % up to 96 h). The *in vivo* analysis performed after their intravenous administration in healthy Wistar rats presented good *in vivo* stability for several days. Encouraging results as well as magnetic and radiochemical properties of ^{177}Lu -PLL-MNPs (80 °C) justify their further testing toward the potential use as theranostic agents for diagnostic and combined radionuclide-hyperthermia therapeutic applications.

1. Introduction

Magnetic nanoparticles are promising nanostructures for application in diagnosis and therapy due to their biocompatibility, simple fabrication technology, and the ability to be manipulated with an external magnetic field (Eivazzadeh-Keihan et al., 2021; Eivazzadeh-Keihan et al., 2020). The development of a theranostic agent is a strategic goal in the field of personalized medicine because just one application enables both diagnostics of cancer at an early stage and then more efficient therapy through a prolonged period (Ahmed et al., 2012). Magnetic nanoparticles have been already proven as a good cancer theranostic agent (Mumtaz et al., 2020; Khizar et al., 2021; Lima-Tenório et al.,

2016) but frequent aggregation and instability in some biological environments limit their broader application. Modification of magnetic nanoparticles' surface by amino acids can improve their physicochemical characteristics and prevent some of the aforementioned shortcomings *in vivo* (Nosrati et al., 2019). Furthermore, the presence of an amino acid on the surface of nanoparticles may ensure biological identity to nanoparticles, therefore they are also noted as smart nanomaterials (Dubey et al., 2015). The magnetic nanoparticles modified with amino acid could be used for numerous biological applications like drug delivery, bioimaging, biosensing, etc. (Pandya et al., 2018) Pandya et al. examined *in vitro* DNA binding, antioxidant, antimicrobial, and anti-cancer assessment of functionalized magnetic nanoparticles with

* Corresponding author at: Laboratory for radioisotopes, Vinča Institute of Nuclear Sciences, University of Belgrade, Mike Petrovića Alasa 12-14, P.O. Box 522, 11001 Belgrade, Serbia.

E-mail address: mmarija@vin.bg.ac.rs (M. Mirković).

<https://doi.org/10.1016/j.ijpharm.2022.122288>

Received 26 July 2022; Received in revised form 3 October 2022; Accepted 8 October 2022

Available online 14 October 2022

0378-5173/© 2022 Elsevier B.V. All rights reserved.

different amino acids such as serine, alanine, cysteine, histidine, and methionine. Amino acids are zwitterionic, hence, the surface charge of amino acid-functionalized nanoparticles can be tailored by varying the pH of the solution. Amino acid lysine is very suitable for biological use due to its non-toxicity, non-antigenicity, good biocompatibility, and biodegradability (Ma et al., 2014). Poly-L-lysine (PLL) is a synthetic biocompatible polymer assembled of the positively charged amino acid lysine and it is broadly used in pharmacy. It was previously used for the modification of magnetic nanoparticles and showed at low concentrations no toxicity, no antigenicity, and good biocompatibility while at higher concentrations exhibited cytotoxic activities in a cell type-dependent manner (tests *in vitro*) (Khmara et al., 2017; Kubovcikova et al., 2019; Antal et al., 2018). The successful synthesis of gold nanoparticles using various amino acids has been reported recently (Marryama et al., 2015; Daima et al., 2013). Tryptophan-coated gold nanoparticles were used to inhibit amyloid aggregation of insulin (Dubey et al., 2015). Proline-coated gold nanoparticles were used as a highly efficient nanocatalyst for the enantioselective direct aldol reaction in water (Khmar et al., 2013). The ability of lysine, glycine, and tryptophan-modified magnetic particles to inhibit lysozyme amyloid fibrillization and destroy amyloid fibrils was also studied and the results revealed that the most effective activities were observed for tryptophan-modified magnetic nanoparticles due to aromatic rings in the structure of amino acid used as a coatings (Antosova et al., 2019). In addition to this role, amino acids though their functional groups provide sites for the attaching of radionuclides, ligands, or specific proteins, thus enabling their wider application.

For several decades, Iodine-131 (^{131}I) has been used in clinical practice in low doses for diagnosis and staging, and in large doses for ablation therapy of thyroid cancer. It represents a typical example of a theranostic radionuclide with very favorable physicochemical characteristics for therapy ($t_{1/2} = 8.02$ days, E_{β} of 0.607 MeV) and γ -ray emission which allows the monitoring of therapy (Hong and Ahn, 2017). Encouraging results of several studies on investigation of the potential of ^{131}I -labeled nanoparticles in cancer treatment support the idea of their application as a multifunctional therapeutic agent combining chemotherapy (PTX) and radiotherapy (^{131}I), or hyperthermia and radiotherapy (^{131}I) (Tian et al., 2017; Stanković et al., 2020). Lutetium-177 (^{177}Lu) (half-life 6.7 days) is the ideal β^- radionuclide for theranostics due to its energy of 497 keV which penetrates 2 mm into the tissues and the accompanying emission of γ -photons of 208 keV (11 %) and 113 keV (6.4 %), used for diagnostic evaluation and dosimetry (Das and Banerjee, 2015). The advantage of the long half-life of ^{177}Lu has been utilized in the radiosynovectomy of knee joints, in the therapy of hepatocellular carcinoma, and for the monitoring of the pharmacokinetics of the potential agents. Several studies were conducted with ^{177}Lu -labeled AuNPs for imaging and therapy in tumor-bearing mice (Yook et al., 2016; Silva et al., 2020). To the best of our knowledge, amino acid-functionalized MNPs were radiolabeled only with diagnostic radionuclide $^{99\text{m}}\text{Tc}$, with the aim to use a combination of multiple imaging and characterization tools such as SPECT and MRI to obtain more sensitive, non-invasive, high-resolution, and quantitative imaging for the early detection of various diseases (Büyükkok et al., 2019). *In vivo* behaviour of tryptophan functionalized magnetic nanoparticles was examined after their labeling with $^{99\text{m}}\text{Tc}$ but studies with therapeutic radionuclides were not done (Mathur et al., 2020).

The present study aimed to design radiolabeled functionalized magnetic nanoparticles for potential theranostic use. MNPs were synthesized by the coprecipitation method, amino acid-functionalized, fully characterized, and then labeled with ^{131}I and ^{177}Lu . Among the tested MNPs, a sample with the best heating power under the AMF, and the highest radiochemical purity and *in vitro* stability, was further analyzed *in vivo* in healthy male Wistar rats, to determine its stability in physiological conditions.

2. Materials and methods

2.1. Materials

Poly-L-lysine hydrobromide ($(\text{C}_6\text{H}_{12}\text{N}_2\text{O})_n \cdot \text{HBr}$; (PLL, $M_w = 150\text{--}300$ kDa)), ferric chloride hexahydrate ($\text{FeCl}_3 \cdot 6\text{H}_2\text{O}$), ferrous sulfate heptahydrate ($\text{FeSO}_4 \cdot 7\text{H}_2\text{O}$), tryptophan (Trp), proline (Pro), perchloric acid (HClO_4), ninhydrin-molybdate reagent, ammonium hydroxide (NH_4OH), 1-ethyl-3-[3-dimethylaminopropyl] carbodiimide hydrochloride (EDC), and 2-[(2-Iodobenzoyl)amino]acetic acid were purchased from Sigma-Aldrich. All solutions were prepared using ultrapure water. Na^{131}I was procured from POLATOM, Poland. Lutetium-177 was obtained from the ITG, Germany ($^{177}\text{LuCl}_3$ in 0.04 M HCl solution). The human serum was purchased from the National Blood Transfusion Institute (Belgrade, Serbia).

Radioactivity of the samples was measured using a dose calibrator (CRC-15R beta, Capintec Inc., Ramsey, New York, USA) while in the quality control, biodistribution, and *in vitro* and *in vivo* studies gamma counter (WIZARD 2480, Perkin Elmer, USA) was used. An imaging study was done by the Bruker Xtreme II instrument.

2.2. Preparation of amino acid-functionalized magnetic nanoparticles

To investigate the possibilities of radiolabeling, two types of magnetic nanoparticles were proposed and synthesized. The first one was with a magnetite core and poly-L-lysine coating, described in detail in our previous study (Khmara et al., 2017; Kubovcikova et al., 2019). Briefly, 2.7 ml of 50 % w/v $\text{FeCl}_3 \cdot 6\text{H}_2\text{O}$ was added to 0.77 g of $\text{FeSO}_4 \cdot 7\text{H}_2\text{O}$ dissolved in distilled water (~10 % w/w). The mixture was stirred in a capped glass vessel until 75 °C was reached. Then, 5 ml of NH_4OH was added and the black precipitate was formed immediately. After 15 min of mixing, the suspension was washed several times and sonicated with an immersion probe ultrasonifier (Branson Ultrasonics Corporation, Danbury, CT, U.S.A.). These unmodified nanoparticles are hereinafter referred to as MNPs. After the determination of magnetite concentration in the suspension, the defined amount of magnetite suspension and PLL solution was mixed, put in a glass vial and sonicated for 5 min in an ice bath under 75 % of power, while the ratio of the components PLL: $\text{Fe}_3\text{O}_4 = 2$ (w/w) was kept. The samples were prepared in multiple smaller batches, washed, and concentrated by centrifugation (30,000 rpm, 1 h). The collected precipitates formed the final sample (PLL-MNPs). The concentration of iron (iron oxide) and PLL content was determined by using UV/Vis spectrophotometry.

The second one consists of electrostatically stabilized iron oxide MNPs modified with amino acids proline and tryptophan. The MNPs stabilized by HClO_4 (hereinafter referred to as MF) were prepared according to our previous study (Antal et al., 2018). The MF surface modification by tryptophan and proline was carried out by a simple adsorption procedure. Briefly, both tryptophan and proline were dissolved in ultrapure water, and the constant volume of Trp (Trp concentration ranging from 0.01 to 9 mg/ml) as well as Pro (Pro concentration ranging from 0.025 to 15 mg/ml) solutions were added to the aqueous suspension of MF. The samples were diluted with ultrapure water to the final volume of 4 ml. The mixtures were stirred at 25 °C for 72 h and centrifuged at 35,000 rpm for 2 h. After ultracentrifugation, supernatants were used to estimate Trp and Pro concentration on magnetic nanoparticle surfaces, and precipitates were collected and dispersed in deionized water to prepare a stock suspension of both Trp (Trp-MF) and Pro (Pro-MF) modified magnetic nanoparticles for the following physicochemical and biological characterization. The part of the stock suspension was lyophilized for thermogravimetric (TG) analysis. The prepared nanoparticles with different amounts of Trp and Pro were prepared in the same way and were fully characterized by different techniques to find out the optimal theoretical loading of Trp and Pro concentration needed to prepare a stable sample for further *in vitro* and *in vivo* testing.

2.3. Physicochemical characterization

UV/Vis spectrophotometry was used to determine the concentration of iron (iron oxides) and PLL, Trp, and Pro. For this purpose, Specord 40 spectrophotometer (Analytic Jena GmbH, Jena, Germany) was applied and the absorbance of investigated samples was measured in a quartz cell with an optical path length of 10 mm. Iron content in MNPs and MF samples was determined by thiocyanate colorimetry described previously (Woods and Mellon, 1941) while the concentration of PLL in the supernatant was determined using the method described by Shen (Shen et al., 1984). The amount of PLL adsorbed on MNPs was calculated from the difference between theoretical loading and PLL remaining in the supernatant after centrifugation. The real PLL: Fe₃O₄ w/w ratio was found to be 0.13 mg PLL to 1 mg of Fe₃O₄. Pro and Trp quantities were also determined in the supernatants obtained after ultracentrifugation of Pro-MF and Trp-MF samples by the slightly modified method of Anantharaman (Anantharaman et al., 2017). The supernatants diluted with citrate buffer (pH 5.6) were allowed to react with ninhydrin-molybdate reagent according to the above-mentioned procedure and their absorbance was measured at 400 and 565 nm. The final Pro and Trp amounts in the Pro-MF and Trp-MF samples were calculated.

The particle size distribution, as well as surface charge of the samples, were measured by using dynamic light scattering (DLS, with a scattering angle of 173° at 25 ± 0.1 °C using disposable zeta cells DTS 1070) and laser doppler electrophoresis using a Zetasizer Nano ZS apparatus (Malvern Instruments, UK). The dispersions were diluted in 10 mM NaCl to give an optimal intensity of ~ 10⁵ counts per second. Prior to measurements, the samples were homogenized in an ultrasonic bath for 10 s, and then 2 min relaxation was allowed. For the zeta potential measurements, the phase analysis light scattering (PALS) method was used. The instrument calculated the zeta potential from the electrophoretic mobility using the Smoluchowski equation (1):

$$\zeta = U\eta/\epsilon \quad (1)$$

where ζ is zeta potential, U electrophoretic mobility, η medium viscosity, and ϵ is dielectric constant. The samples for surface charge measurements were diluted in the same solvent (10 mM NaCl). The number of repeat measurements performed on the samples was 3 and a pause of 60 s was between repeat measurements to minimize Joule heating and electrode polarization effects.

Transmission electron microscope JEOL-TEM 2100F (TEM) operated at 200 kV was used to acquire electron micrographs for size and shape description. Dilute water dispersions of the iron oxide nanoparticles were distributed over carbon-coated TEM grids and analyzed. Size distributions of the nanoparticles were determined by measuring the edge length (or diameter) of 500–600 particles of each sample.

The disc centrifuge particle size analyzer based on the differential centrifugal sedimentation (DCS) technique (Model DC24000 UHR, CPS Instruments Inc., Prairieville, LA, USA) equipped with a 405 nm laser for the detection and running at 24,000 rpm was utilized to perform the particle size analysis. A dilute sample (<1% solid content) was injected into the center of the hollow spinning disc partly filled with density gradient solution. The disc centrifuge physically separates the nanoparticles and then measures them as they pass a light source detector. The time for particles to reach the detector beam versus beam intensity is converted to a size distribution using both Stokes' Law (modified slightly for use in a centrifuge) and Mie theory light scattering calculations. Results are expressed as the arithmetic mean of the volume-weighted particle distributions.

The magnetization studies were conducted by MPMS3 SQUID magnetometer (Quantum Design GmbH, Darmstadt Germany). $M-H$ curves of solid samples were measured at 300 K and saturation magnetization (M_s) and coercive field (H) were evaluated.

Thermogravimetric analysis was applied to estimate the amino acid amount in the prepared amino-functionalized MNPs. Measurements

were carried out using TGDTA Setaram SETSYS 16 analyzer for washed and freeze-dried samples with different amino acid (Pro, Trp) to MNPs (w/w) ratios. Weight losses were measured under air from room temperature up to 600 °C with a rate of 10 °C·min⁻¹.

2.4. Measurements in an alternating and non-alternating magnetic field

Specific absorption rate (SAR) of Pro-MF, Trp-MF, and PLL-MNPs dispersed in water (with MNPs concentration 6 mg/ml) was determined using a commercial AC applicator (DM100 series, nB nanoscale Biomagnetics, Spain) at the resonant frequency of 252 kHz and field amplitude of 15.9 kA/m. The calorimetric curves were monitored in an alternating magnetic field (AMF) for 6 min. The SAR values of the measured samples have been evaluated by a linear curve fitting in the first 30 s of the heating curves $(dT/dt)_0$ by a corrected slope method to correct any linear losses (Wildeboer et al., 2014) using the equation (2):

$$SAR(W/g) = c_{NP} + \frac{\rho_1}{\rho_{NP}} \times c_1 \times \left(\frac{dT}{dt} \right)_{max} \quad (2)$$

In (2) c_{NP} is the specific heat of the nanoparticles (J/(kg·K)), ρ_{NP} is the density of the colloid (kg/m³), ρ_1 is the density of the dispersing agent (kg/m³) and $(dT/dt)_{max}$ is calorimetric curve temperature gradient (K/s). ILP (Intrinsic Loss Power) was calculated from SAR using the equation (3):

$$ILP(nHm^2/kg) = SAR/H_0^2 f \quad (3)$$

in which f represents the frequency of the applied magnetic field (Hz), while H_0 is magnetic field amplitude (A/m).

For the analysis of the sample in non-alternating external magnetic field, device constructed in our laboratory was used (Kuraica et al., 2018). Sanyo laser diode DL5147-040 in the single mode regime at wavelength $\lambda = 655$ nm was applied. Transmitted laser light was measured with a photodiode.

2.5. Radiolabeling with ¹³¹I

To form a covalent bond between the Iodine-131 Hippuran and Pro-MF, Trp-MF, and PLL-MNPs, the carbodiimide method using ethyl-3-(3-dimethylaminopropyl)carbodiimide (EDC) was applied (Zhang et al., 2007). Iodine-131 Hippuran was prepared by the method described in the literature (Mitta et al., 1961). Briefly, the functionalized magnetic nanoparticle samples with an iron oxide concentration of 6 mg/ml were washed twice with 1 ml of 0.1 M 2-(*N*-Morpholino) ethanesulfonic acid (MES) buffer using a neodymium magnet for pellet precipitation after each washing step. After washing, the samples were resuspended in freshly prepared 1 ml MES buffer containing 10–15 mg EDC and were mixed at room temperature for 10 min. Iodine-131 Hippuran was added to the functionalized samples (approximately 50 μ Ci, 1.85 MBq) and the suspension was mixed on a shaker at room temperature for 2 h. Iodine-131 Hippuran conjugated with functionalized MNPs was separated from the supernatant by magnetic decantation. To determine the radiolabeling yield (RLY), activities of supernatant and pellet were measured in a gamma counter. The pellet was resuspended in 3 ml of 0.9 % NaCl. It is expected that only Iodine-131 hippuran conjugated to functionalized MNPs would be found in the pellet after magnetic separation. At the same time, unbound Iodine-131 Hippuran and possibly free ¹³¹I, as a product of radiolysis of Iodine-131 Hippuran, would remain in the supernatant.

Radiochemical purity (RCP) of Iodine-131 Hippuran conjugated to functionalized magnetic nanoparticles samples was performed after purification and resuspension of the pellet, using TLC chromatography with 85 % methanol as the mobile phase and ITLC-SG as the stationary phase. With this method, remained unbound Iodine-131 Hippuran moved with the front ($R_f = 0.9-1.0$) while Iodine-131 Hippuran conjugated to functionalized MNPs stayed at the origin ($R_f = 0.0-0.1$).

The radiochemical purity was calculated using equations:

$$\%^{131}\text{I labeled conjugate} = (\text{counts of }^{131}\text{I labeled conjugate area} / \text{total counts of strip}) \times 100 \quad (4)$$

$$\% \text{ unbound Iodine-}^{131}\text{ Hippuran} = (\text{counts of bound Iodine-}^{131}\text{Hippuran at the front} / \text{total counts of strip}) \times 100 \quad (5)$$

2.6. Radiolabeling with ^{177}Lu

For the labeling of Pro-MF, Trp-MF, and PLL-MNPs samples with ^{177}Lu , a direct method was used (Radović et al., 2015; Ognjanović et al., 2019). ^{177}Lu was added to the samples (approximately 50 μCi , 1.85 MBq) and the suspension was mixed on a shaker at two different temperatures (room temperature and 80 °C) and pH 4.5–5 for 1 h. RLY of the magnetic nanoparticles labeled with ^{177}Lu was not possible to determine due to their high stability, and hence magnetic separation was not possible. RCP of ^{177}Lu labeled functionalized magnetic nanoparticles was determined using thin-layer chromatography on silica gel - SG strips (ITLC-SG) and 0.1 M acetate buffer as the mobile phase. With this method, unbound $^{177}\text{Lu}^{3+}$ moved with the front ($R_f = 0.8\text{--}0.9$) while ^{177}Lu -labeled functionalized MNPs stayed at the origin ($R_f = 0.0\text{--}0.1$). After completing the development, strips were dried, cut into 1 cm segments, and radioactivity measured in a gamma counter.

The radiochemical purity was calculated using equations:

$$\%^{177}\text{Lu - labeled functionalized MNPs} = (\text{counts of }^{177}\text{Lu - labeled functionalized MNPs area} / \text{total counts of strip}) \times 100 \quad (6)$$

$$\% \text{ free }^{177}\text{Lu} = (\text{counts of free }^{177}\text{Lu at the front} / \text{total counts of strip}) \times 100 \quad (7)$$

2.7. In vitro stability studies

The stability studies were performed by measuring the release of ^{131}I and ^{177}Lu from the radiolabeled functionalized magnetic nanoparticles during their incubation in 1 ml of saline (0.9 % NaCl, pH = 7.3) or human serum at 37 °C up to 96 h. At several time points after the radiolabeling ($t = 24, 48, 72, \text{ and } 96 \text{ h}$), samples were analyzed using the above-mentioned radiochromatography methods.

2.8. Biodistribution and imaging

Biodistribution of radiolabeled functionalized MNPs was studied in healthy male Wistar rats (100 \pm 10 g body weight, 4 weeks old, on three to five animals per one-time point, "Vinča" Institute of Nuclear Sciences). Radiolabeled functionalized magnetic nanoparticles in a volume of 0.1 ml were injected intravenously via a tail vein (approx. 0.5–1.0 MBq per animal). Three hours after the injection, two Wistar rats were anesthetized with ketamine/xylazine (80–100/10 mg/kg i.p.) and imaged on a Bruker Xtreme II instrument using two modalities: X-ray and radiation. After imaging, these Wistar rats were sacrificed along with others at predetermined time points ($t = 0.5, 3, 24, \text{ and } 96 \text{ h}$) via spinal cord dislocation. The organs of interest and samples of blood (1 ml) were sorted, weighed, and measured for radioactivity in the gamma counter. The uptake into the organs was presented as a percentage of the injected activity per organ (% ID/organ) when compared with appropriate standards for injected dose (ID). All animal experimental data are expressed as average \pm standard deviation (SD) from each group. All experiments were performed in compliance with the National animal welfare law and EU Directive 2010/63/EU, permission No. 323-07-

04725/2018-05, and were approved by the Ethical committee of

the "Vinča" Institute of Nuclear Sciences.

3. Results and discussion

3.1. Preparation of optimized formulation of Pro, Trp and PLL modified magnetic nanoparticles

In order to find out the optimum Trp and Pro amount adsorbed on MNPs, several sets of samples with various theoretical weight ratios of Trp and Pro/MNPs were prepared and characterized by different techniques.

The batch of samples with Pro to MNPs w/w ratios ranging from 0.5 to 30 was prepared, centrifuged, and studied using UV/Vis spectrophotometry to find out the optimum Pro/MNPs weight ratio. As can be seen in Fig. 1a, the adsorption efficiency, calculated as a ratio of the actual adsorbed amount of Pro to theoretical loading Pro amount expressed in %, reaches saturation at Pro/MNP ratio 5 w/w indicating

that maximally ~ 17 % of theoretical Pro loading amount can be adsorbed onto MNPs. These results are relatively in good coincidence with outcomes from the TG analysis. By estimating the TG curves of the samples with different theoretical weight ratios of Pro/MNPs, the amount of Pro adsorbed on MNPs was determined, and consequently, the adsorption efficiency was also calculated. As can be seen in inset Fig. 1a, the same optimal weight ratio Pro/MNPs = 5 was found from TG analysis. Thus, the sample Pro-MF with optimal input weight ratio Pro/MNPs = 5, and the adsorption efficiency of ~ 17 % was selected as the optimized formulation for the following tests (referred to as Pro-MF).

In the case of the preparation of optimized formulation of Trp-MF, DLS and TG analysis were used. Fig. 1b shows zeta potential dependency on different input weight ratios Trp/MNPs ranging from 0.5 to 15 and the determination of the optimal theoretical loading of Trp weight ratio to MNPs. As seen in the figure the absolute value of zeta potential decreases with increasing the weight ratio Trp/MNPs. Having fitted the experimental data, the optimal Trp/MNPs weight ratio was found to be about 7. The outcome was confirmed using TG measurements as well (Fig. 1b, inset). On the basis of the obtained results, the Trp-MF sample with a theoretical loading ratio of Trp/MNPs = 7 and adsorption efficiency ~ 3.5 % was chosen as the optimized formulation for the following experiments.

The previously synthesized, optimized, and characterized PLL-MNPs sample, described in detail in our papers (Khmara et al., 2017; Kubovickova et al., 2019), was suggested as the third sample for *in vitro* and *in vivo* experiments.

Prior to *in vitro* and *in vivo* experiments, the selected samples with optimum input weight ratio of Pro/MNPs = 5 (Pro-MF), Trp/MNPs = 7 (Trp-MF), and PLL/MNPs = 2 (PLL-MNPs) were characterized in terms

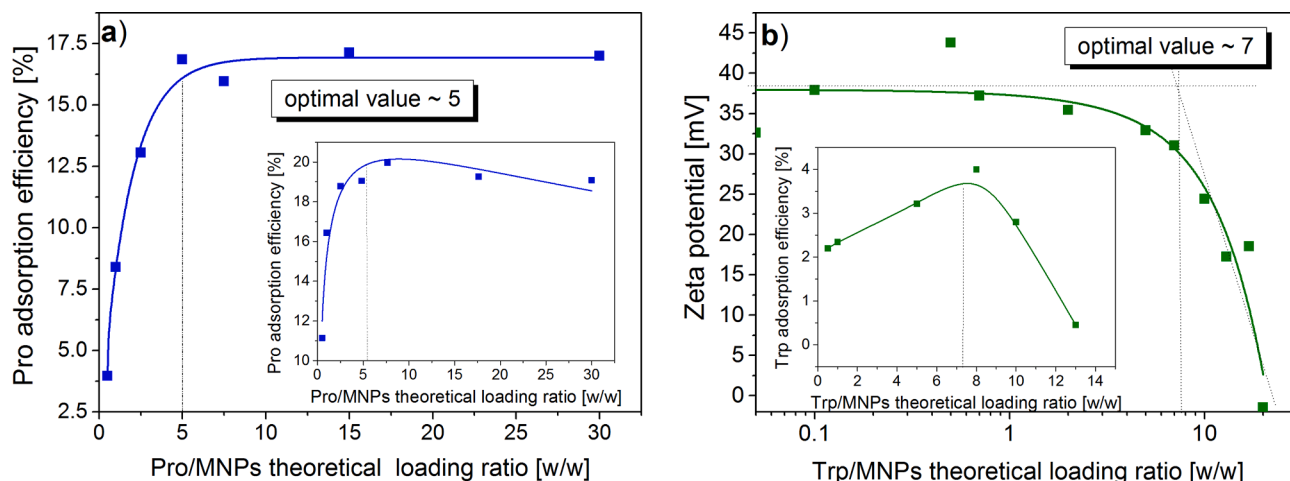
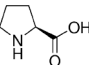
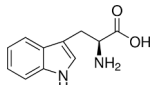
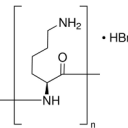


Fig. 1. Effect of various theoretical Pro loading weight ratio on adsorption efficiency determined from UV/Vis measurements (a). Effect of various theoretical Trp loading weight ratio on zeta potential (b). Insets are Pro (a) and Trp (b) adsorption efficiency obtained from TG analysis.

Table 1

Overview of the physicochemical characteristics of unmodified and proline, tryptophan and poly-L-lysine modified iron oxide nanoparticles.

	SAMPLE				
	MF	Pro-MF	Trp-MF	MNPs	PLL-MNPs
Modifier	–	Proline	Tryptophan	–	Poly L-lysine
Modifier formula	–			–	
Modifier/MNPs optimal ratio	–	5	7	–	2
D_{HYDR} [nm]	34.2 ± 0.4	41.5 ± 0.3	49.7 ± 0.5	91.2 ± 3.4	112.6 ± 0.3
PDI	0.138	0.227	0.322	0.256	0.114
Zeta potential [mV]	$+23.8 \pm 1.8$	$+28.6 \pm 1.5$	$+25.0 \pm 1.8$	$+18 \pm 1.7$	$+34.4 \pm 0.9$
IEP	6.9	6.05	6.03	6.7	10.8
D_{DCS} [nm]	27.3 ± 0.5	53.8 ± 0.4	58.5 ± 0.5	103.4 ± 2.1	107.8 ± 0.6
D_{TEM} [nm]	7.5 ± 0.1	8.5 ± 0.3	8.6 ± 0.1	10.1 ± 0.4	11.1 ± 1.0
M_S [emu/g] at 300 K	60.6 ± 0.2	53.4 ± 0.1	47.1 ± 0.1	75.6 ± 0.4	57.2 ± 0.2
D_{MAG} [nm]	9.61 ± 0.10	9.59 ± 0.07	10.02 ± 0.06	9.28 ± 0.15	9.89 ± 0.10
Modifier/MNPs [mg/mg] _{SQUID}	–	0.14	0.29	–	0.32
Modifier/MNPs [mg/mg] _{TGA}	–	0.19	0.25	–	0.13

Modifier/MNPs optimal ratio – optimal modifier/MNPs input weight ratio; D_{HYDR} – hydrodynamic diameter of particles; PDI – polydispersity index; zeta potential – Zeta potential of dispersions diluted in 10 mM NaCl; IEP – isoelectric point (the pH value at which the zeta potential equals zero); D_{DCS} – mean values from weight size distributions obtained by differential centrifugal sedimentation measurements; D_{TEM} – mean size of magnetic nanoparticles; M_S – saturation magnetization at 300 K; D_{MAG} – magnetic core diameter determined from magnetic measurements; Modifier/MNPs_{SQUID} – ratio determined from SQUID measurements; Modifier/MNPs_{TGA} – ratio determined from TG analysis.

of morphology, size distribution, surface, and magnetic properties (see Table 1).

3.2. Physicochemical characterization of PLL, pro and Trp modified magnetic nanoparticles

There are numerous analytical techniques, for example, TEM, DLS, DCS, and thermomagnetic methods employed to measure the size/size distribution of the samples. TEM is one of the most powerful analytical tools available, which can give direct structural and morphological information about magnetic nanoparticles. Using the short wavelengths (achievable with highly accelerated electrons), it is possible to investigate the structure of MNPs down to the atomic level in detail. Moreover, by TEM micrograph image analysis, it can be determined the size distribution of the MNPs.

Kapitha Fig. 2a-d shows typical TEM images of as-prepared magnetic nanoparticles of MF, Pro-MF, Trp-MF and PLL-MNPs. Particle agglomeration occurs during the preparation (drying) of colloidal stable fluids for TEM investigation. TEM observations revealed an irregular shape of

magnetic nanoparticles. From several images, the histogram with the log-normal fit was constructed for each sample. The core diameter of MF (Fig. 2a), Pro-MF (Fig. 2b), and Trp-MF (Fig. 2c) samples with average sizes between 7 and 9 nm was determined. These values are in good agreement with the results from the magnetic core size estimation according to the Chantrell method (Chantrell et al., 1978). Using this method the magnetic diameters of 9 and 10 nm were obtained.

The core diameter of PLL-MNPs (Fig. 2d) determined from TEM images was around 11 nm. While the image analysis on the TEM micrographs gives the ‘true diameter’ of the particle core (though determined on a statistically small sample), DLS provides the hydrodynamic diameter of particles. The hydrodynamic diameter is the diameter of a sphere that has the same diffusion coefficient within the same viscous environment of the particles being measured and includes both the particle core and adsorption layer. The normalized intensity size distributions of PLL-MNPs, and MF unmodified and MF modified with Pro and Trp obtained by DLS are shown in Fig. 2. As seen in PLL-MNPs size distribution (Fig. 2d), there is a sharp peak at 112.6 nm, which is attributed to the hydrodynamic size of the individual, dispersed

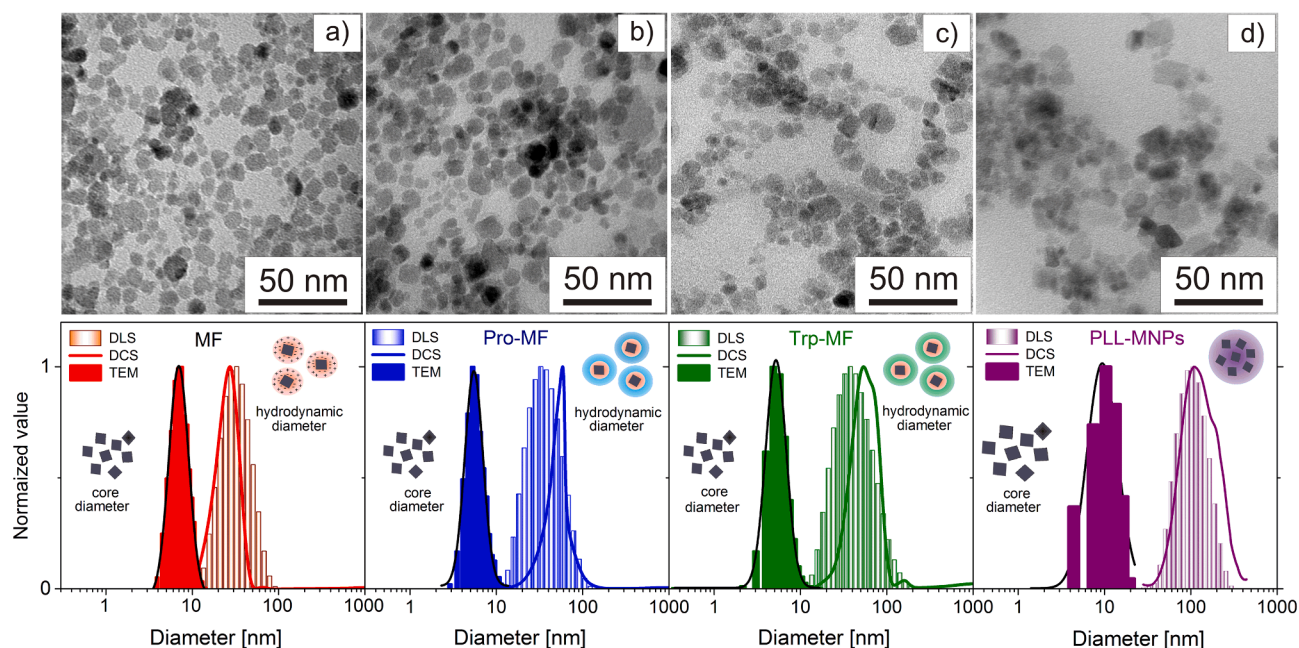


Fig. 2. TEM image of MF (a), Pro-MF (b), and Trp-MF (c), PLL-MNPs (d) samples (upper row) with corresponding size distributions obtained by TEM, DLS and DCS analysis (lower row). In the size distributions images, the normalized value means the normalized count evaluated from TEM images, the normalized intensity for DLS measurements, and normalized weight determined by DCS measurements.

nanoparticles. Fig. 2a-c displays sharp peaks at 34.2 nm, 41.5 nm, and 49.7 nm for samples MF, Pro-MF, and Trp-MF. The values of hydrodynamic diameter (D_{HYDR}) and polydispersity index (PDI) are summarized in Table 1. These values of D_{HYDR} are very close to values of D_{DCS} diameters of 27.3 nm (MF), 53.8 nm (Pro-MF), and 58.5 nm (Trp-MF) obtained by DCS instrument. The increase in size reflects the binding of the amino acids on the magnetic nanoparticles. The uncoated MNPs undergo aggregation resulting in larger nanoparticles' hydrodynamic size ($D_{HYDR} = 91.2$ nm) and PDI = 0.256. In the PLL-MNPs samples, PLL coating avoided the aggregation of nanoparticles which is supported by the lower PDI (0.114) of the coated nanoparticles. The larger size of PLL-MNPs can be caused not only by the larger size of the PLL molecules but also by the fact that PLL can create three-dimensional (3D) structures due to their high hydrophilicity, abundant functional groups, and flexible molecular backbone (Wu et al., 2017).

Zetasizer Nano ZS was also used to measure the surface charge of the selected samples. As the surface charge of particles affects their physical state in fluids (e. g. stability) and thus their interactions with biological systems (e. g. protein absorption), it is necessary to determine the zeta potential values of particles intended for biomedical applications. The

zeta potentials of the selected samples are summarized in Table 1. The increased value of zeta potential of modified samples in comparison with MF and naked MNPs confirms the amino acid adsorption on MF and MNPs surfaces. In addition, the high value of zeta potential of these functionalized MNPs and MF indicates their good colloidal stability in 10 mM NaCl. The absolute zeta potential values of >25 mV are ideal to provide good kinetic stability at room temperature when the particles are stabilized through purely electrostatic interaction (Barick et al., 2014).

The magnetic measurements of the functionalized samples (Pro-MF, Trp-MF, and PLL-MNPs) are shown in Fig. 3. At 300 K, superparamagnetic behavior was observed in all measured samples. The samples did not exhibit hysteresis, i.e. neither coercivity nor remanence (Fig. 3, upper left insets). The saturation magnetizations (M_s) of samples were found to be 53.41, 47.11, and 57.17 emu/g for the Pro-MF, Trp-MF, and PLL-MNPs samples, respectively.

The magnetization decrease, in comparison with unmodified MF and MNPs (see Table 1), is due to the fact that the magnetization is proportional to the weight of the same magnetic material. Increasing the coating layer (in our case Pro, Trp, and PLL) increases the amount of

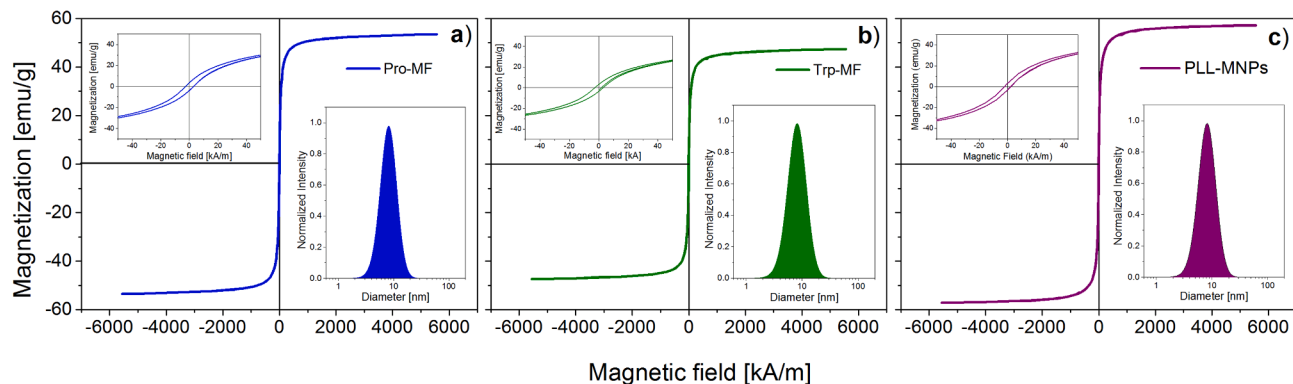


Fig. 3. Hysteresis loops of Pro-MF (a), Trp-MF (b), and PLL-MNPs (c) samples measured at 300 K. Upper left inset: detail of the magnetization curves showing negligible the coercive fields and magnetic remanences. Lower right insets represent magnetic size distributions.

nonmagnetic material (organic) on iron oxide (inorganic). It means that the more organic layer of the coating, the less the amount of iron oxide contained in the same weight of the powdered sample. Next, through dividing saturation magnetization of the samples by the saturation magnetization of unmodified magnetic nanoparticles (MF = 60.6 emu/g, and MNPs = 75.6 emu/g), the iron oxide content in the modified samples can be estimated, which almost corresponds with the results of the TGA analysis.

In addition, the magnetic core diameters (D_{MAG}) of all the prepared samples, which were determined from the fitting of the magnetization M versus magnetic field H curves, are close to those estimated from the TEM measurements (see Table 1).

3.3. Measurements in an alternating and non-alternating magnetic field

Under the influence of an external AC magnetic field, magnetic nanoparticles generate heat and dissipate it into local tumor tissues as a clinically desirable temperature window (between 42 °C and 46 °C) thus inducing apoptosis in the surrounding malignant cells (Dulińska-Litewka et al., 2019; Ramasamy et al., 2018).

The temperature increases of Pro-MF, Trp-MF, and PLL-MNPs in aqueous dispersions (with iron oxide concentration of 6 mg/ml) as a function of the time were determined by exposing them to AMF at a field strength of 15.9 kA/m and frequency of 252 kHz, within the biological limit of $H \cdot f$ product (Fig. 4a). The calculated values of SAR and ILP for all the tested samples are indicated in Table 2. The transformation of magnetic energy into heat depends not only on the field parameters but also on particle structure, their chemical composition, surface modifiers, and the viscosity of the suspending medium. All these parameters determine the SAR value of the samples (Rosensweig, 2002; Illés et al., 2018). Among the synthesized samples, PLL-MNPs presented in the maximum SAR and ILP values (99.7 W/g and 1.56 nH·m²/kg, respectively). The obtained values of PLL-MNPs indicate that these kind of amino acid-functionalized MNPs are capable of generating a sufficient amount of heat, which makes them suitable for hyperthermia-based cancer treatment. The heat generated in the other two samples (Pro-MF and Trp-MF) is modest (see Table 2).

The analysis of samples in a non-alternating magnetic field has been carried out at 400 mT and the results are depicted in Fig. 4b. In previous studies, we have shown that based on the shape of the curves obtained, the effect of hyperthermia can be explained and predicted. The heating capacity of the sample correlates with the depth and width of the well. Generally speaking, the shallower the well, and the greater the jump in transparency, the more pronounced effect of hyperthermia is expected. In certain cases, however, when the sample is very dilute or its magnetic

Table 2

SAR and ILP values of Pro-MF, Trp-MF, and PLL-MNPs ($H_0 = 15.9$ kA/m, $f = 252$ kHz).

Samples	SAR[W/g]	ILP [nH·m ² /kg]
Pro-MF	47.9	0.75
Trp-MF	55.7	0.87
PLL-MNPs	99.7	1.56

properties are not sufficiently pronounced, the well cannot be observed. Such specimens have a very low heating capacity. Even at a field of 400 mT, the samples Trp-MF and Pro-MF do not show any effect, i.e., the absence of a well is noticeable, and the saturation transparency is only slightly higher than the initial one. The appearance of the well and the significant value of transparency at the point of saturation have been noticed only in the case of PLL-MNPs. These results are in complete agreement with the obtained SAR values shown in Table 2, and also with hysteresis loops of Pro-MF, Trp-MF, and PLL-MNPs samples measured at 300 K, where the most pronounced magnetization of 57.17 emu/g has been obtained for PLL-MNPs. The applied frequency and amplitude of the AC field used in these measurements are based on the literature data ($H_0 = 15.9$ kA/m, $f = 252$ kHz). The proper frequency and amplitude of the AC field safe enough for clinical use have not been determined yet. Therefore, in the absence of better criteria, it is necessary to be guided by paper of Atkinson et al. (Atkinson et al., 1984) in which the upper limit on $f \cdot H$ product was given as $4.85 \cdot 10^8$ Am⁻¹s⁻¹. The “Brezovich criterion” was deduced from experiments on healthy patients, subjected to a 13.5 MHz AC field for an hour, and is based on patients’ subjective feelings. Generally speaking, the upper limit of the $f \cdot H$ product can be moved up in the case of smaller volumes treated, shorter field application periods, and depending on the seriousness of the illness. The optimal criterion can’t be a general number, but rather the choice of numbers depending on different parameters, e.g., illness seriousness, tumor size, accessibility, the therapeutic efficacy of continuous and pulsed fields, etc. These parameters and corresponding field-frequency criteria can be determined only through clinical trials. Barring that, the criterion is artificial and has limited usefulness. Furthermore, our tests of the samples in a non-alternating magnetic field show unequivocally that PLL-MNPs are a candidate for a potential application. The method itself has been examined in detail in our previous works (Radović et al., 2021).

3.4. Radiolabeling with ¹³¹I

The process of radiolabeling involves radionuclide attachment to the

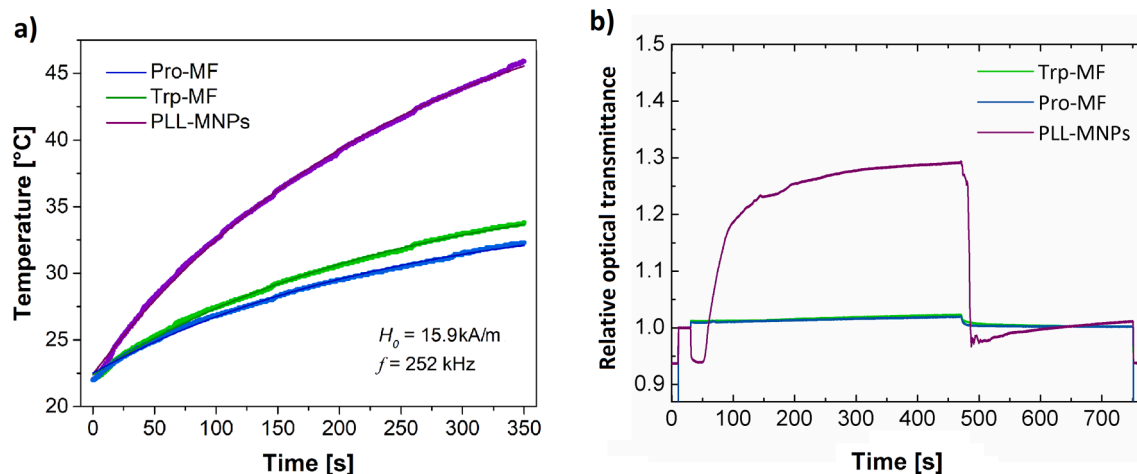
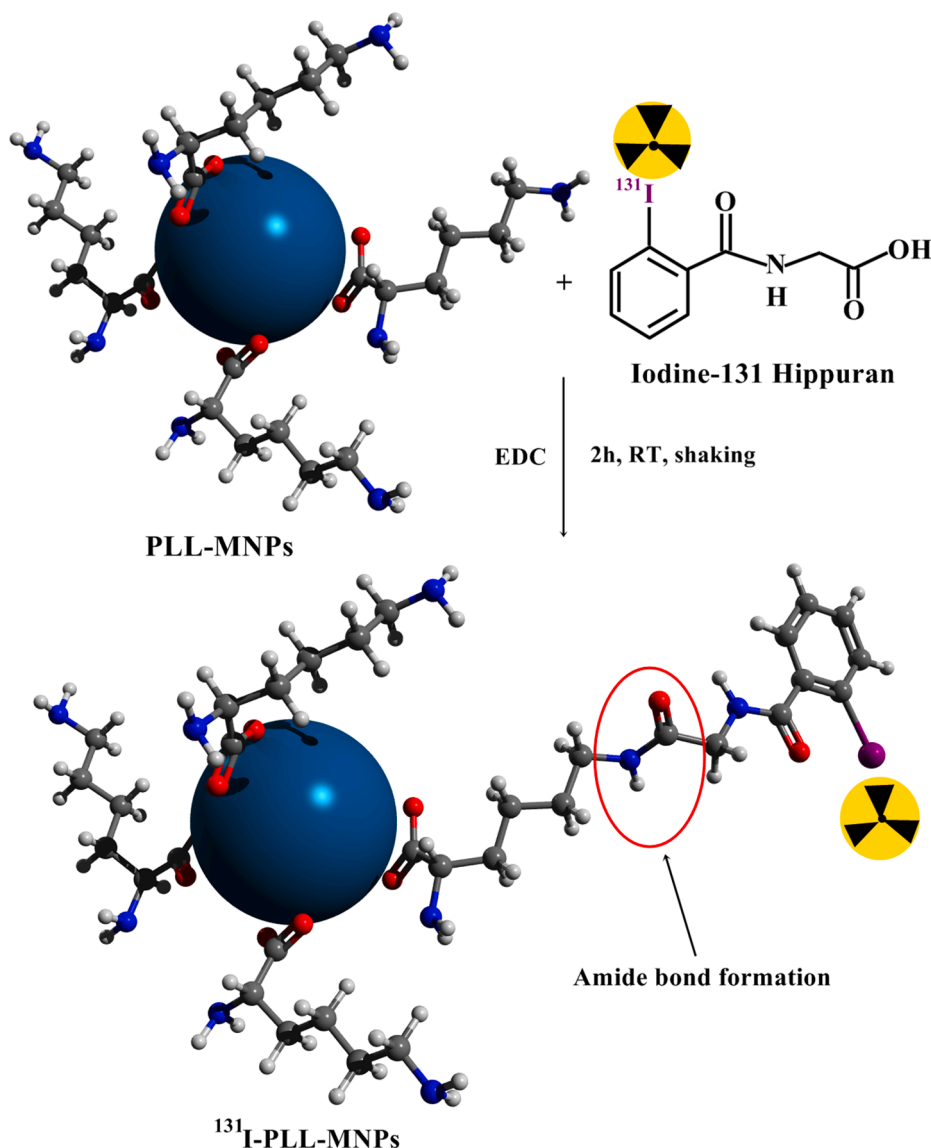


Fig. 4. The temperature increase of Pro-MF, Trp-MF, and PLL-MNPs at magnetic field strength of 15.9 kA/m and frequency of 252 kHz, calorimetric method (a), Time dependence of transmitted diode laser light ($\lambda = 655$ nm) for investigated specimens at magnetic field strength 400 mT (b).



Scheme 1. Radiolabeling of PLL-MNPs with ^{131}I . Due to simplicity, the binding of the lysine monomer is presented.

Table 3

Radiolabeling yield and radiochemical purity of ^{131}I -samples.

^{131}I -samples	RLY	RCP
^{131}I - PLL-MNPs	61.0 ± 1.2	98.8 ± 1.1
^{131}I - Trp-MF	17.1 ± 0.9	–
^{131}I - Pro-MF	11.5 ± 0.6	–

targeting molecule either directly or via the use of some other compounds or a bifunctional chelating agent. Radiolabeling of Pro-MF, Trp-MF, and PLL-MNPs with ^{131}I was performed by indirect method via Iodine-131 Hippuran using the carbodiimide method with EDC which is a high carboxyl- and amine-reactive cross-linker for the coupling^{20,31}. [Scheme 1](#) shows the procedure of PLL-MNPs radiolabeling with ^{131}I .

Measurements of radioactivity in the pellet with ^{131}I -labeled nanoparticles and supernatant after magnetic decantation showed satisfactory (61 %) RLY and very high RCP (98.8 %) only for ^{131}I -PLL-MNPs, while RLY of ^{131}I -Trp-MF and ^{131}I -Pro-MF samples was very low and therefore RCP purity was not determined ([Table 3](#)). These results for RLY were expected because the amino groups-rich PLL on MNPs are suitable for the conjugation with free carboxyl groups of Iodine-131

Hippuran, while proline and tryptophan are without that structural advantage.

3.5. Radiolabeling with ^{177}Lu

The chemistry of trivalent radiometals such as ^{68}Ga , ^{177}Lu , and ^{90}Y allows facile radiolabeling of different molecules either directly or through bifunctional chelators ([Martell and Smith, 1982](#)). The macrocyclic DOTA (1,4,7,10-tetraazacyclododecane-1,4,7,10-tetraacetic acid), one of the most commonly used chelators, forms complexes of lanthanides with significantly high thermodynamic stability and kinetic inertness. However, labeling reactions by DOTA are generally performed at high temperatures under acidic pH and involve long reaction times, which might result in the decomposition of the corresponding protein ligand or entire radioactive complex ([Iori et al., 2017](#)). Direct radiolabeling without the chelating agent is possible by binding of trivalent radiometals to various free functional groups (phosphates, phosphonates, carboxyl, amino, etc.) of the compounds or coatings in the case of functionalized magnetic nanoparticles ([HÁfeli U. Radioactive Microspheres for Medical Applications., 2001](#)). At pH 5, lutetium is mainly in the form of Lu^{3+} ions suitable for radiolabeling, while the concentration of hydrolyzate is very low ([López-González et al., 2007](#)).

At this pH, only amino groups of amino acids (coatings), protonated at pH 5, and thus positively charged, remain free and available for binding because negatively charged carboxylate groups have already been used for binding to the iron of MNPs. If the strongly basic conditions (above pH 9), where most of the amino groups are deprotonated, would be applied for radiolabeling, the concentration of free Lu^{3+} ions is substantially lower due to their hydrolysis and radiolabeling would not be possible. Therefore, although it would be expected that PLL-MNPs having the highest positive value of zeta potential, do not bind or weakly bind Lu^{3+} ions, the results of radiolabeling show the highest radiolabeling yield exactly for these coatings. It is assumed that due to the acid-base equilibrium, a small percentage of deprotonated amino groups that exist at pH 5, allows the binding of very low concentrations of Lu^{3+} ions but that was sufficient to achieve a high radiolabeling yield. As PLL has a large number of amino groups that may potentially bind ions, the highest probability of binding of Lu^{3+} ions is in the case of PLL-MNPs.

For the radiolabeling of all samples (Pro-MF, Trp-MF, and PLL-MNPs) with $^{177}\text{LuCl}_3$, mild conditions in terms of temperature were first examined (room temperature), and then it was increased to 80 °C. Scheme 2 shows the procedure of PLL-MNPs radiolabeling with ^{177}Lu .

Determination of RLY of ^{177}Lu -labeled samples using magnetic decantation was not possible due to their exceptional stability. Therefore, their RCP was determined using ITLC-SG immediately after the radiolabeling. PLL-MNPs radiolabeled at both examined temperatures have much higher radiochemical purity than other samples (Table 4), hence they were only used for *in vitro* studies.

3.6. *In vitro* and *in vivo* stability investigations

Radiolabeled samples must be stable long enough to avoid the release and accumulation of free radionuclides in healthy tissues and organs and side effects in them and reduced therapeutical effects.

In vitro stability is tested only for ^{131}I and ^{177}Lu radiolabeled samples with high radiochemical purity. *In vitro* stability results of ^{177}Lu -PLL-MNPs (radiolabeled at 80 °C) incubated in saline (Fig. 5a) and human serum (Fig. 5b) at 37 °C for 96 h, indicate their great stability. Even after 96 h, this radiolabeled agent showed stability higher than 98 % in both tested mediums. The stability of ^{177}Lu -PLL-MNPs (RT) is above 80 % during the tested period. The stability of ^{131}I -PLL-MNPs in saline and serum rapidly decreased over time (from 96.23 % and 93.67 % at 24 h to 76.26 % and 72.24 % at 96 h in saline and serum, respectively), so it was declared unsuitable for the use in therapy. Therefore, only ^{177}Lu -PLL-MNPs (80 °C) were selected for further *in vivo* testing on experimental animals.

The biodistribution of ^{177}Lu -PLL-MNPs (80 °C) was studied in healthy Wistar rats using the radiotracer technique (Fig. 5c). The

Table 4

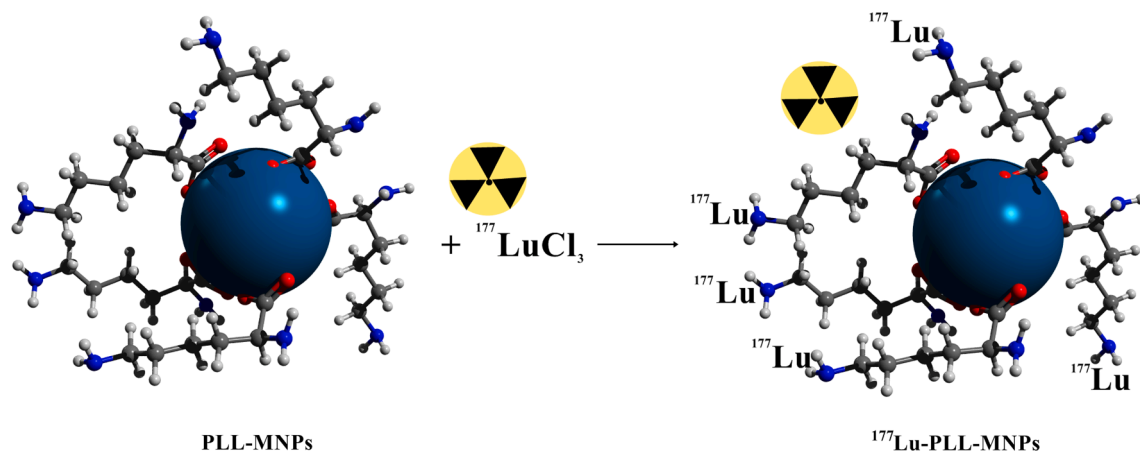
Radiochemical purity of samples after ^{177}Lu -labeling at different temperatures.

^{177}Lu -samples	RCP, RT, %	RCP, 80 °C, %
^{177}Lu - PLL-MNPs	99.00 ± 0.57	99.00 ± 0.88
^{177}Lu - Trp-MF	45.66 ± 1.03	70.38 ± 1.23
^{177}Lu - Pro-MF	59.57 ± 0.63	69.24 ± 0.98

biodistribution was observed at four-time points ($t = 0.5, 3, 24,$ and 96 h) by measuring radioactivity in tissues and/or organs after intravenous administration of ^{177}Lu -PLL-MNPs (80 °C). The highest accumulation of ^{177}Lu -PLL-MNPs (80 °C) was observed in the liver (from 69.45 %ID at 0.5 h after administration to 84.30 %ID at 96 h), followed by the spleen (from 15.90 %ID at 0.5 h after administration to 9.62 %ID at 96 h), while the very low amount of ^{177}Lu -PLL-MNPs (80 °C) was found in the rest of tissues/organs (Fig. 5c). Such results are expected because nanoparticles of these characteristics (with the special influence of size) fast clear from the systemic circulation, mainly by the action of the liver and splenic macrophages. Functionalization of MNPs with PLL notably contributed to an increase *in vivo* stability compared to bare MNPs by preventing the formation of micrometer-sized particles, which was confirmed by small lung uptake (8.80 %ID after 0.5 h and 1.65 %ID after 96 h). Insignificant radioactivity was measured in the skeleton (femur), a target organ for most metals including ^{177}Lu , indicating that ^{177}Lu was strongly bound to the PLL-MNPs and did not exist in the free form.

4. Conclusions

In this study, two types of magnetic nanoparticles were synthesized and functionalized with proline, tryptophan, and poly-L-lysine to obtain agents with properties suitable for hyperthermia and radiotherapy. For the first time, amino acid modified magnetic particles were labeled with radionuclides ^{131}I and ^{177}Lu that could be used both for diagnosis and therapy. Radiolabeling of Trp-MF and Pro-MF with ^{131}I by indirect radiolabeling via Iodine-131 Hippuran was with very low RLY (less than 20 %) in accordance with the amino groups-rich PLL-MNPs suitable for the conjugation with free carboxyl groups of Iodine-131 Hippuran (61 %). Unfortunately, the stability of ^{131}I -PLL-MNPs in saline and serum rapidly decreased over time, so it was unsuitable for further *in vivo* testing. Similar results for the radiolabeling were obtained after direct labeling of samples with ^{177}Lu since, in contrast to Pro and Trp, PLL has a large number of available amino groups that may potentially bind ^{177}Lu , and therefore PLL-MNPs both radiolabeled at room and elevated temperature showed high radiochemical purity (99 %) measured just after the radiolabeling. However, only poly-L-lysine functionalized MNPs obtained by radiolabeling at 80 °C expressed high *in vitro* stability and high *in vivo* stability (up to 96 h). Additionally, SAR value for poly-L-



Scheme 2. Radiolabeling of PLL-MNPs with ^{177}Lu . Due to simplicity, the binding of the lysine monomer is presented.

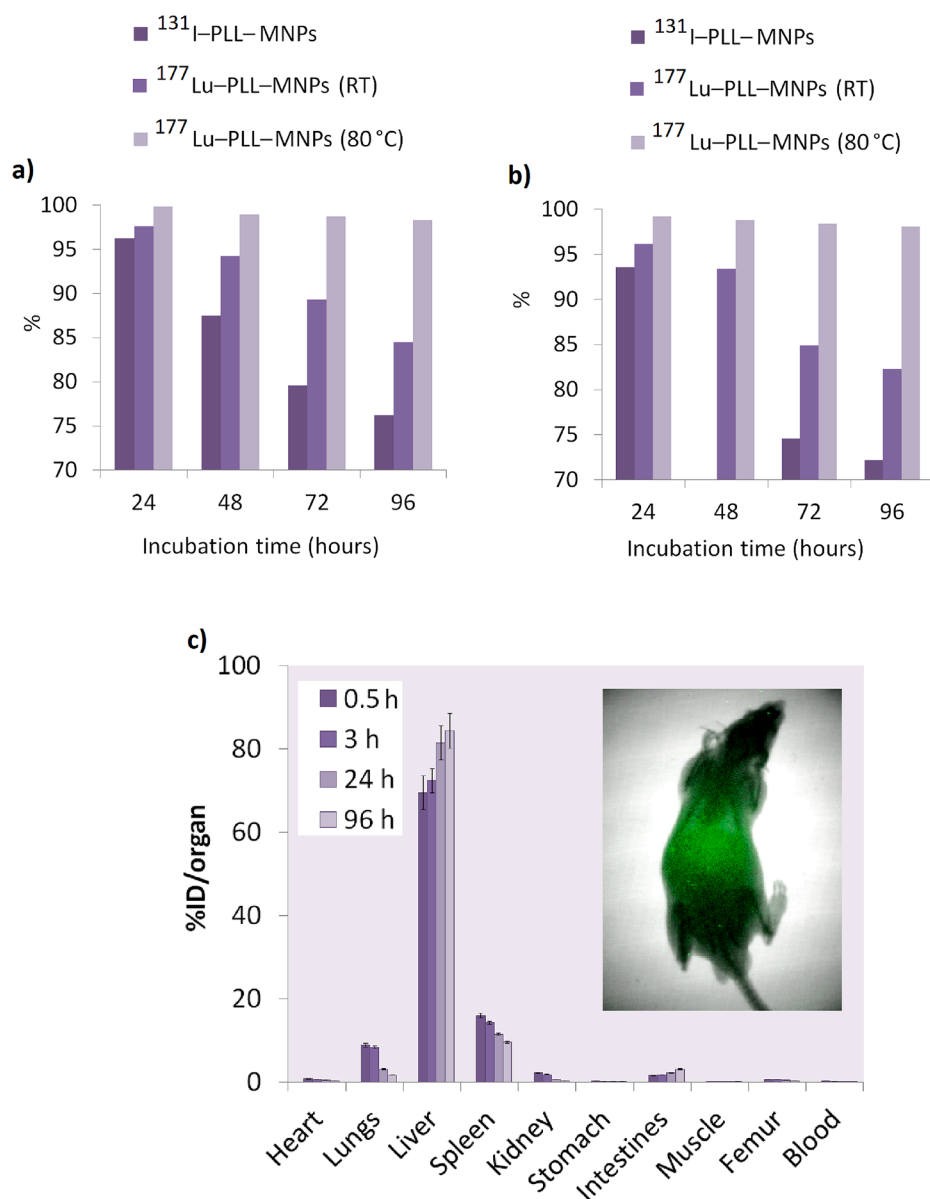


Fig. 5. *In vitro* stability of ¹³¹I-PLL-MNPs, ¹⁷⁷Lu-PLL-MNPs (RT) and ¹⁷⁷Lu-PLL-MNPs (80 °C) in: saline (a) and human serum (b) after incubation at 37 °C during 96 h. Biodistribution results of ¹⁷⁷Lu-PLL-MNPs (80 °C) in different tissues after 0.5, 3, 24, and 96 h of intravenous administration in healthy Wistar rats. The results are expressed as %ID per organ (the mean of three to five rats ± standard deviations). The inset shows radio imaging on Wistar rat 96 h after i.v. injection of ¹⁷⁷Lu-PLL-MNPs (80 °C) (c).

lysine functionalized MNPs shows their high potential for the possible application in hyperthermia. The results on healthy Wistar rats suggest that future research should exploit the full potential of ¹⁷⁷Lu-PLL-MNPs (80 °C) for hyperthermia-based cancer treatment in combination with radioactivity on tumor-bearing mice, predominantly using intratumoral administration.

5. Availability of data and material

The data that support the findings of this study are available on request from the corresponding author.

CRedit authorship contribution statement

Marija Mirković: Conceptualization, Methodology, Writing – original draft. **Zorana Milanović:** Investigation, Formal analysis, Writing – original draft. **Marko Perić:** Investigation, Software, Data curation. **Sanja Vranješ-Đurić:** Writing – review & editing, Funding acquisition. **Miloš Ognjanović:** Investigation, Writing – original draft. **Bratislav Antić:** Resources, Project administration. **Milorad Kuraica:** Methodology, Investigation. **Ivan Krstić:** Investigation. **Martina Kubovcikova:**

Resources, Formal analysis, Writing – original draft. **Iryna Antal:** Data curation, Visualization. **Radka Sobotova:** Methodology, Investigation. **Vlasta Zavisova:** Funding acquisition, Validation, Writing – review & editing. **Alena Jurikova:** Investigation. **Martin Fabian:** Resources, Formal analysis. **Martina Koneracka:** Methodology, Investigation, Supervision.

Declaration of Competing Interest

The authors declare that they have no known competing financial interests or personal relationships that could have appeared to influence the work reported in this paper.

Data availability

Data will be made available on request.

Acknowledgements

To our dear friend and colleague Dr. Aleksandar S. Nikolić. The research was supported by the Ministry of Education, Science and

Technological Development of the Republic of Serbia (contract numbers 451-03-68/2022-14/200017, 451-03-68/2022-14/200162) and through funding the VINCENT Center of Excellence. The work was also supported by the Slovak Research and Development Agency under contracts Nos. APVV-14-0120, APVV-SK-SRB-18-0055, APVV-DS-FR-19-0052, by the Slovak Science Grant Agency VEGA - Project No. 2/0033/19 and by the Operational Programme Integrated Infrastructure, project "NANOVIR", ITMS: 313011AUW7, and "BIOVID-19", ITMS 313011AVG3 co-funded by ERDF.

References

- Ahmed, N., Fessi, H., Elaissari, A., 2012. Theranostic applications of nanoparticles in cancer. *Drug Discov Today*. 17 (17–18), 928–934. <https://doi.org/10.1016/j.drudis.2012.03.010>.
- Anantharaman, S., Padmarajiah, N., Al-Tayar, N.G.S., Shrestha, A.K., 2017. Ninhydrin-sodium molybdate chromogenic analytical probe for the assay of amino acids and proteins. *Spectrochim. Acta Part A Mol. Biomol. Spectrosc.* 173, 897–903. <https://doi.org/10.1016/j.saa.2016.10.040>.
- Antal, I., Koneracka, M., Kubovcikova, M., Zavisova, V., Khmara, I., Lucanska, D., Jelenska, L., Vidlickova, I., Zaticovicova, M., Pastorekova, S., Bugarova, N., Micusik, M., Omastova, M., Kopcansky, P., 2018. d, l-lysine functionalized Fe₃O₄ nanoparticles for detection of cancer cells. *Colloids Surf B Biointerfaces*. 163, 236–245. <https://doi.org/10.1016/j.colsurfb.2017.12.022>.
- Antosova, A., Bednarikova, Z., Koneracka, M., Antal, I., Marek, J., Kubovcikova, M., Zavisova, V., Jurikova, A., Gazova, Z., 2019. Amino acid functionalized superparamagnetic nanoparticles inhibit Lysozyme Amyloid fibrillation. *Chem. – A Eur. J.* 25 (31), 7501–7514. <https://doi.org/10.1002/chem.201806262>.
- Atkinson, W.J., Brezovich, I.A., Chakraborty, D.P., 1984. Usable frequencies in hyperthermia with thermal seeds. *IEEE Trans. Biomed. Eng.* BME-31 (1), 70–75. <https://doi.org/10.1109/TBME.1984.325372>.
- Barick, K.C., Singh, S., Bahadur, D., Lawande, M.A., Patkar, D.P., Hassan, P.A., 2014. Carboxyl decorated Fe₃O₄ nanoparticles for MRI diagnosis and localized hyperthermia. *J. Colloid Interface Sci.* 418, 120–125. <https://doi.org/10.1016/j.jcis.2013.11.076>.
- Büyükkök, O., Uçar, E., İçhedef, Ç., Çetin, O., Teksöz, S., 2019. Bioevaluation of ^{99m}Tc(I) carbonyl-radiolabeled amino acid coated magnetic nanoparticles *in vivo*. *Mater. Chem. Phys.* 235, 121751 <https://doi.org/10.1016/j.materchemphys.2019.121751>.
- Chantrell, R.W., Popplewell, J., Charles, S.W., 1978. Measurements of particle size distribution parameters in ferrofluids. *IEEE Trans. Magn.* 14 (5), 975–977. <https://doi.org/10.1109/TMAG.1978.1059918>.
- Daima, H.K., Selvakannan, P.R., Shukla, R., Bhargava, S.K., Bansal, V., 2013. Fine-Tuning the Antimicrobial Profile of Biocompatible Gold Nanoparticles by Sequential Surface Functionalization Using Polyoxometalates and Lysine. *PLoS One*. 8(10), e79676. doi:10.1371/JOURNAL.PONE.0079676.
- Das, T., Banerjee, S., 2015. Theranostic Applications of Lutetium-177 in Radionuclide Therapy. *Curr Radiopharm.* 9 (1), 94–101. <https://doi.org/10.2174/1874471008666150313114644>.
- Dubey, K., Anand, B.G., Badhwar, R., Bagler, G., Navya, P.N., Daima, H.K., Kar, K., 2015. Tyrosine- and tryptophan-coated gold nanoparticles inhibit amyloid aggregation of insulin. *Amino Acids* 47 (12), 2551–2560. <https://doi.org/10.1007/S00726-015-2046-6>.
- Dulińska-Litewka, J., Łazarczyk, A., Hałubiec, P., Szafranski, O., Karnas, K., Karewicz, A., 2019. Superparamagnetic Iron Oxide Nanoparticles—Current and Prospective Medical Applications. *Mater* 12(4), 617. doi:10.3390/MA12040617.
- Eivazzadeh-Keihan, R., Bahojb Noruzi, E., Khanmohammadi Chenab, K., Jafari, A., Radinekiyan, F., Hashemi, S.M., Ahmadvour, F., Behboudi, A., Mosafar, J., Mokhtarzadeh, A., Maleki, A., Hamblin, M.R., 2020. Metal-based nanoparticles for bone tissue engineering. *J. Tissue Eng. Regen. Med.* 14 (12), 1687–1714. <https://doi.org/10.1002/term.3131>.
- Eivazzadeh-Keihan, R., Bahreiniazad, H., Amiri, Z., et al., 2021. Functionalized magnetic nanoparticles for the separation and purification of proteins and peptides. *TRAC Trends Anal Chem.* 141, 116291. doi:10.1016/j.trac.2021.116291.
- HÄfeli, U., 2001. Radioactive Microspheres for Medical Applications. 213–248. doi:10.1007/0-306-46891-3_9.
- Hong, C.M., Ahn, B.C., 2017. Redifferentiation of radioiodine refractory differentiated thyroid cancer for reapplication of I-131 therapy. *Front. Endocrinol. (Lausanne)* 8 (OCT), 260. <https://doi.org/10.3389/FENDO.2017.00260/BIBTEX>.
- Illés, E., Szekeres, M., Tóth, I.Y., Szabó, Á., Iván, B., Turcu, R., Vékás, L., Zupkó, I., Jaics, G., Tombác, E., 2018. Multifunctional PEG-carboxylate copolymer coated superparamagnetic iron oxide nanoparticles for biomedical application. *J. Magn. Magn. Mater.* 451, 710–720. <https://doi.org/10.1016/j.jmmm.2017.11.122>.
- Iori, M., Capponi, P.C., Rubagotti, S., et al., 2017. Labelling of ⁹⁰Y- and ¹⁷⁷Lu-DOTA-bioconjugates for targeted radionuclide therapy: A comparison among manual, semiautomated, and fully automated synthesis. *Contrast Media Mol. Imaging* 2017, 1–12. <https://doi.org/10.1155/2017/8160134>.
- Khair, N., Navas, R., Elhalem, E., Valdivia, V., Fernández, I., 2013. Proline-coated gold nanoparticles as a highly efficient nanocatalyst for the enantioselective direct aldol reaction in water. *RSC Adv.* 3 (12), 3861–3864. <https://doi.org/10.1039/C3RA22955F>.
- Khizar, S., Ahmad, N.M., Zine, N., Jaffrezic-Renault, N., Errachid-El-Salhi, A., Elaissari, A., 2021. Magnetic Nanoparticles: From Synthesis to Theranostic Applications. *ACS Appl Nano Mater.* 4 (5), 4284–4306. https://doi.org/10.1021/ACSANM.1C00852/ASSET/IMAGES/MEDIUM/AN1C00852_0012.GIF.
- Khmara, I., Koneracka, M., Kubovcikova, M., Zavisova, V., Antal, I., Csach, K., Kopcansky, P., Vidlickova, I., Csaderova, L., Pastorekova, S., Zaticovicova, M., 2017. Preparation of poly-L-lysine functionalized magnetic nanoparticles and their influence on viability of cancer cells. *J. Magn. Magn. Mater.* 427, 114–121. <https://doi.org/10.1016/j.jmmm.2016.11.014>.
- Kubovcikova, M., Koneracka, M., Strbak, O., Molcan, M., Zavisova, V., Antal, I., Khmara, I., Lucanska, D., Tomco, L., Barathova, M., Zaticovicova, M., Dobrota, D., Pastorekova, S., Kopcansky, P., 2019. Poly-L-lysine designed magnetic nanoparticles for combined hyperthermia, magnetic resonance imaging and cancer cell detection. *J. Magn. Magn. Mater.* 475, 316–326. <https://doi.org/10.1016/j.jmmm.2018.11.027>.
- Kuraica, M.M., Iskrenović, P., Perić, M., Krstić, I., Nikolić, A.S., 2018. External magnetic field influence on magnetite and cobalt-ferrite nano-particles in ferrofluid. *Chem. Pap.* 72 (6), 1535–1542. <https://doi.org/10.1007/s11696-017-0380-8>.
- Lima-Tenório, M.K., Pineda, E.A.G., Ahmad, N.M., Agusti, G., Manzoor, S., Kabbaj, D., Fessi, H., Elaissari, A., 2016. Aminodextran polymer-functionalized reactive magnetic emulsions for potential theranostic applications. *Colloids Surf B Biointerfaces*. 145, 373–381. <https://doi.org/10.1016/j.colsurfb.2016.05.020>.
- López-González, H., Jiménez-Reyes, M., Solache-Ríos, M., Rojas-Hernández, A., 2007. Solubility and hydrolysis of lutetium at different [Lu³⁺] initial. *J. Radioanal. Nucl. Chem.* 274 (1), 103–108. <https://doi.org/10.1007/S10967-006-6910-4>.
- Ma, Y.H., Peng, H.Y., Yang, R.X., Ni, F., 2014. Preparation of Lysine-Coated Magnetic Fe₂O₃ Nanoparticles and Influence on Viability of A549 Lung Cancer Cells. *Asian Pacific J Cancer Prev.* 15 (20), 8981–8985. <https://doi.org/10.7314/APJCP.2014.15.20.8981>.
- Martell, A.E., Smith, R.M., 1982. Critical Stability Constants. *Crit. Stab. Constants*. <https://doi.org/10.1007/978-1-4615-6761-5>.
- Maruyama, T., Fujimoto, Y., Maekawa, T., 2015. Synthesis of gold nanoparticles using various amino acids. *J. Colloid Interface Sci.* 447, 254–257. <https://doi.org/10.1016/j.jcis.2014.12.046>.
- Mathur, R., Chauhan, R.P., Singh, G., Singh, S., Varshney, R., Kaul, A., Jain, S., Mishra, A. K., 2020. Tryptophan conjugated magnetic nanoparticles for targeting tumors overexpressing indoleamine 2,3 dioxygenase (IDO) and L-type amino acid transporter. *J. Mater. Sci. - Mater. Med.* 31 (10) <https://doi.org/10.1007/S10856-020-06438-X>.
- Mitta, A.E.A., Fraga, A., Veall, N., 1961. A simplified method for preparing I-131-labelled Hippuran. *Int. J. Appl. Radiat. Isot.* 12 (3–4), 146–147. [https://doi.org/10.1016/0020-708X\(61\)90076-X](https://doi.org/10.1016/0020-708X(61)90076-X).
- Mumtaz, T., Qindeel, M., Asim, ur.Rehman, Tarhini, M., Ahmed, N., Elaissari, A., 2020. Exploiting proteases for cancer theranostic through molecular imaging and drug delivery. *Int. J. Pharm.* 587, 119712. doi:10.1016/j.jlpharm.2019.119712.
- Nosrati, H., Hamzehei, H., Afroogh, S., Ashabi, S.F., Attari, E., Manjili, H.K., 2019. Phenyl alanine & Tyrosine Amino acids Coated Magnetic Nanoparticles: Preparation and Toxicity study. *Drug Res (Stuttg.)* 69 (5), 277–283. <https://doi.org/10.1055/A-0664-0431>.
- Ognjanović, M., Radović, M., Mirković, M., Prijović, Ž., Puerto Morales, M.D., Čeh, M., Vranješ-Đurić, S., Antić, B., 2019. ^{99m}Tc-, ⁹⁰Y-, and ¹⁷⁷Lu-labeled Iron oxide nanoflowers designed for potential use in dual magnetic hyperthermia/radionuclide cancer therapy and diagnosis. *ACS Appl. Mater. Interfaces* 11 (44), 41109–41117. <https://doi.org/10.1021/acsami.9b16428>.
- Pandya, S.R., Patel, S., Bakshi, S., Singh, M., 2018. *In vitro* DNA binding, antioxidant, antimicrobial and anticancer assessment of amino acid functionalized magnetic nanoparticles. *Appl. Surf. Sci.* 451, 1–19. <https://doi.org/10.1016/j.apsusc.2018.04.190>.
- Radović, M., Calatayud, M.P., Goya, G.F., Ibarra, M.R., Antić, B., Spasojević, V., Nikolić, N., Janković, D., Mirković, M., Vranješ-Đurić, S., 2015. Preparation and *in vivo* evaluation of multifunctional ⁹⁰Y-labeled magnetic nanoparticles designed for cancer therapy. *J. Biomed. Mater. Res. Part A* 103 (1), 126–134. <https://doi.org/10.1002/jbm.a.35116>.
- Radović, M., Mirković, M., Nikolić, A.S., Kuraica, M., Iskrenović, P., Milanović, Z., Vranješ-Đurić, S., Perić, M., 2021. Transmittance measurements in non-alternating magnetic field as reliable method for determining of heating properties of phosphate and phosphonate coated Fe₃O₄ magnetic nanoparticles. *J. Inorg. Organomet. Polym.* 31 (11), 4426–4433. <https://doi.org/10.1007/S10904-021-02059-1>.
- Ramasamy, T., Ruttala, H.B., Sundaramoorthy, P., Poudel, B.K., Youn, Y.S., Ku, S.K., Choi, H.-G., Yong, C.S., Kim, J.O., 2018. Multimodal selenium nanoshell-capped Au@mSiO₂ nanopatform for NIR-responsive chemo-photothermal therapy against metastatic breast cancer. *NPG Asia Mater.* 10 (4), 197–216. <https://doi.org/10.1038/s41427-018-0034-5>.
- Rosensweig, R.E., 2002. Heating magnetic fluid with alternating magnetic field. *J. Magn. Magn. Mater.* 252, 370–374. [https://doi.org/10.1016/S0304-8853\(02\)00706-0](https://doi.org/10.1016/S0304-8853(02)00706-0).
- Shen, W.C., Yang, D., Ryser, H.J.P., 1984. Colorimetric determination of microgram quantities of polylysine by trypan blue precipitation. *Anal. Biochem.* 142 (2), 521–524. [https://doi.org/10.1016/0003-2697\(84\)90500-1](https://doi.org/10.1016/0003-2697(84)90500-1).
- Silva, F., Campello, M.P.C., Paulo, A., 2020. Radiolabeled Gold Nanoparticles for Imaging and Therapy of Cancer. *Mater* 14(1), 4. doi:10.3390/MA14010004.
- Stanković, A., Mihailović, J., Mirković, M., Radović, M., Milanović, Z., Ognjanović, M., Janković, D., Antić, B., Mijović, M., Vranješ-Đurić, S., Prijović, Ž., 2020. Aminosilanized flower-structured superparamagnetic iron oxide nanoparticles coupled to ¹³¹I-labeled CC49 antibody for combined radionuclide and hyperthermia therapy of cancer. *Int. J. Pharm.* 587, 119628 <https://doi.org/10.1016/j.ijpharm.2020.119628>.

- Tian, L., Chen, Q., Yi, X., Wang, G., Chen, J., Ning, P., Yang, K., Liu, Z., 2017. Radionuclide I-131 labeled Albumin-Paclitaxel nanoparticles for synergistic combined chemo-radioisotope therapy of cancer. *Theranostics*. 7 (3), 614–623. <https://doi.org/10.7150/THNO.17381>.
- Wildeboer, R.R., Southern, P., Pankhurst, Q.A., 2014. On the reliable measurement of specific absorption rates and intrinsic loss parameters in magnetic hyperthermia materials. *J. Phys. D Appl. Phys.* 47 (49), 495003 <https://doi.org/10.1088/0022-3727/47/49/495003>.
- Woods, J.T., Mellon, M.G., 1941. Thiocyanate Method for Iron: A Spectrophotometric Study. *Ind Eng Chem - Anal Ed.* 13 (8), 551–554. <https://doi.org/10.1021/1560096A013>.
- Wu, J., Chen, Y., Wang, Y.u., Yin, H., Zhao, Z., Liu, N., Xie, M., Chen, Y., 2017. Poly-L-lysine brushes on magnetic nanoparticles for ultrasensitive detection of Escherichia coli O157: H7. *Talanta* 172, 53–60. <https://doi.org/10.1016/J.TALANTA.2017.05.035>.
- Yook, S., Cai, Z., Lu, Y., Winnik, M.A., Pignol, J.P., Reilly, R.M., 2016. Intratumorally injected ¹⁷⁷Lu-labeled gold nanoparticles: Gold nanoseed Brachytherapy with application for Neoadjuvant treatment of locally advanced breast cancer. *J. Nucl. Med.* 57 (6), 936–942. <https://doi.org/10.2967/JNUMED.115.168906>.
- Zhang, S., Bian, Z., Gu, C., Zhang, Y.u., He, S., Gu, N., Zhang, J., 2007. Preparation of anti-human cardiac troponin I immunomagnetic nanoparticles and biological activity assays. *Colloids Surf B Biointerfaces*. 55 (2), 143–148. <https://doi.org/10.1016/J.COLSURFB.2006.11.041>.